

3–D Secular Dynamics of the ν Andromedae Planetary System

T.A. Michtchenko, S. Ferraz-Mello,
Instituto de Astronomia, Geofísica e Ciências Atmosféricas, USP
Rua do Matão 1226, 05508-900 São Paulo, Brazil
E-mail: tatiana@astro.iag.usp.br

and C. Beaugé
Observatorio Astronómico, Universidad Nacional de Córdoba, Laprida 854, (X5000BGR)
Córdoba, Argentina

- Total number of pages: 32
- Number of manuscript pages: 20
- Number of figures: 9
- Number of tables: 1

Proposed running head: 3-D Dynamics of the v Andromedae System

Editorial correspondence to:

Tatiana A. Michtchenko
Instituto de Astronomia, Geofísica e Ciências Atmosféricas
Universidade de São Paulo
Rua do Matão, 1226
São Paulo, Brasil 05508-900
Email: tatiana@astro.iag.usp.br

Abstract

The three-dimensional secular behavior of a system composed of a central star and two massive planets is modeled semi-analytically in the frame of the general three-body problem. We apply the analysis to the case of the two outer planets in the ν Andromedae system. The topology of the 3-D phase space of this system is investigated in detail by means of surfaces of section, topological and dynamical mapping techniques. We obtain the general structure of its secular phase space, and the boundaries of its spatial secular stability. We find that this system is secularly stable in a large domain of eccentricities and inclinations.

Several regimes of motion of the ν Andromedae system are observed. With respect to the secular angle $\Delta\varpi$, there are possible circulations, oscillations (around 0 and 180°), and high eccentricity/inclination librations in secular resonances. With respect to the secular angle ω_1 , there are possible direct circulation and high inclination libration around $\pm 90^\circ$ in the secular resonance. The regions of transition between domains of different regimes of motion are characterized by chaotic motion.

Key words: Celestial mechanics; Extrasolar planets; Planetary dynamics; Resonances

1 Introduction

The discovery of extra-solar planets has brought into focus a long standing, but poorly understood problem in Celestial Mechanics, namely the long-term stability of planetary systems. In fact, the dynamical evolution of our Solar system has been the object of exhaustive studies for at least two centuries, but its stability is not yet completely understood. The extra-solar systems provoke our imagination by their unusual configurations, which include Jupiter-mass planets at very small semi-major axes and unexpectedly large eccentricities, and raise new questions in our understanding of their dynamical stability.

The first studies on the long-term stability of these systems has been done in the form of direct numerical integrations of the full equations of motion. In the last years, a large number of papers were published applying this approach to several planetary systems, in order to investigate their dynamical aspects. The numerical integration over very-long time intervals is a powerful approach for exploring the dynamical features of the systems with two and more planets. However, the correct interpretation of the results of numerical investigations is not simple and should be always founded on the basic concepts provided by analytical or semi-analytical investigations. Only analytical approaches are able to explore the whole parameter space of the problem and provide the ultimate answer on the question of the global stability of the system under study.

In the preceding paper (Michtchenko and Malhotra 2004, hereafter referred to as MM2004), we developed a new semi-analytical approach, consisting of a numerical averaging over the short-period perturbations in the mutual interaction of the two planets on coplanar orbits. In such a way, we obtained the secular Hamiltonian and applied the results of the analysis to the case of the system of the two outer planets, **C** and **D**, of ν Andromedae system. Our analysis showed that the secular behavior of the ν Andromedae system is stable over a large domain of eccentricities, which is bounded by the collision curve defined by close approaches between two planets. Below the collision curve, secular instabilities occur in the vicinity of nonlinear secular resonance, a new dynamical feature in planetary systems discovered in our nonlinear analysis. In addition, the analytical approach allowed us to understand such common features of planetary systems as the coupled apsidal line motion with aligned and anti-aligned orientations.

The present paper extends the study to the non-coplanar secular motion of the planets. It is known that, at present, the majority of the discovered extra-solar systems are spatially unresolved. In fact, the spectroscopic radial velocity technique measures only the line-of-sight component of the velocity of the star and the fitting of Keplerian eclipses is unable to detect the inclinations and nodes of the planetary orbits. The system must be observed over a large number of orbital periods, in order to allow a full N-body fit to be able to determine all the orbital parameters of the system (Ferraz-Mello *et al.* 2005). The exceptions are the multi-planet systems of strongly interacting companions involved in mean-motion resonances. Presently, only the two planets, **B** and **C**, around PSR B1257+12, which are near the 3:2 mean-motion resonance, have the individual orbital inclinations determined (Konacki and Wolszczan 2003).

It is expected that astrometric and photometric techniques contribute to the task of complete characterization of known systems (e.g. the masses and the spatially resolved orbital elements). In analogy with the unusual planar orbital parameters of the known extra-solar systems, the elements to be determined may have spatial characteristics that are hard to explain within the context of current theoretical models based on the Laplace-Lagrange secular theory (Veras and Armitage 2004). We should be prepared to face this new challenge. This is the aim of the present paper.

The paper is organized as follows. In section 2, we introduce the 3-D model and describe the basic concepts of the general three-body problem which allow us to reduce a number of degrees of freedom of the Hamiltonian system to 2. In section 3, we apply this approach to obtain geometrical pictures of the secular phase space of the ν Andromedae system. The topology and dynamical maps of the representative subspaces of initial conditions of this system are presented in the section 4. In sections 5 and 6, we study the dependence of the secular dynamics on the magnitudes of the Angular Momentum Deficit and the initial mutual inclination between the orbital planes of the planets, respectively. In section 7, we explore the neighborhood of the ν Andromedae system searching for the mean-motion resonances in this region. We provide a summary of our results in section 8. Finally, in the Appendix we briefly describe the numerical techniques used.

2 The 3-D model

The Hamiltonian which describes the motion of the 3-body system in the heliocentric reference frame can be written, using Poincaré canonical variables, as

$$H = \underbrace{\sum_{i=1}^2 \left(\frac{\vec{p}_i^2}{2m'_i} - \frac{\mu_i m'_i}{|\vec{r}_i|} \right)}_{\text{Keplerian part}} - \underbrace{\frac{G m_1 m_2}{\Delta}}_{\text{direct part}} + \underbrace{\frac{(\vec{p}_1 \cdot \vec{p}_2)}{m_0}}_{\text{indirect part}}, \quad (1)$$

where \vec{r}_i and $\vec{p}_i = m_i \frac{d\vec{\rho}_i}{dt}$ are the planet position vectors relative to the star and their conjugate momenta, respectively; $\vec{\rho}_i$ are the position vectors relative to the center of gravity of the three-body system. G is the gravitational constant, $\mu_i = G(m_0 + m_i)$, $m'_i = m_i m_0 / (m_0 + m_i)$ and $\Delta = |\vec{r}_1 - \vec{r}_2|$. Hereafter, the indices $i = 1, 2$ stand for the inner and outer planets, respectively.

Associated with the Keplerian part of the Hamiltonian, a set of mass-weighted Delaunay's elliptic variables is introduced as

$$\begin{aligned} M_i &= \text{mean anomaly}, & L_i &= m'_i \sqrt{\mu_i a_i}, \\ \omega_i &= \text{argument of pericenter}, & G_i &= L_i \sqrt{1 - e_i^2}, \\ \Omega_i &= \text{longitude of node}, & H_i &= L_i \sqrt{1 - e_i^2} \cos I_i, \end{aligned}$$

where a_i , e_i and I_i are the canonical heliocentric semi-major axes, eccentricities and inclinations of the planets, respectively. The relationship between canonical and usual osculating heliocentric orbital elements is described in detail in Ferraz-Mello *et al.* (2004). In the canonical variables, the Hamiltonian (1) can be written as

$$H = - \sum_{i=1}^2 \frac{\mu_i^2 m_i'^3}{2 L_i^2} - \frac{G m_1 m_2}{a_2} R(L_i, G_i, H_i, M_i, \omega_i, \Omega_i), \quad (2)$$

where the sum describes Keplerian motions of the planets and R is the disturbing function.

To study the secular behavior of the system, we perform numerically the averaging of the Hamiltonian (2) with respect to the mean anomalies of the planets. The description of the numerical averaging procedure can be found in (MM2004). The secular Hamiltonian is then defined by

$$\overline{H}_{\text{sec}} = - \frac{1}{(2\pi)^2} \int_0^{2\pi} \int_0^{2\pi} \frac{G m_1 m_2}{a_2} R(L_i, G_i, H_i, M_i, \omega_i, \Omega_i) dM_1 dM_2, \quad (3)$$

where the Keplerian part is constant and therefore need not be considered.

After the elimination of the short periodic terms, the averaged Hamiltonian $\overline{H}_{\text{sec}}$ does not depend on M_1 and M_2 ; consequently, L_1 and L_2 (thus a_1 and a_2) are constant in time. It is worth emphasizing that, due to the scissors' kind of the averaging used, the semi-major axes are constant only up to the first order in the planetary masses; this consideration is important to bear in mind when the results of the model are compared to those obtained through purely numerical integrations.

The secular Hamiltonian $\overline{H}_{\text{sec}}$ given by Eq. 3 has four degrees of freedom and eight variables remain in the averaged problem. However, based on the conservation of the total angular momentum, we can reduce the problem by two degrees of freedom. This reduction is known as the elimination of the nodes (Jacobi 1842).

For this purpose, we perform the canonical transformation of the nodes to

$$\begin{aligned}\theta_1 &= \frac{\Omega_1 + \Omega_2}{2}, & J_1 &= H_1 + H_2 = L_1 \sqrt{1 - e_1^2} \cos I_1 + L_2 \sqrt{1 - e_2^2} \cos I_2, \\ \theta_2 &= \frac{\Omega_1 - \Omega_2}{2}, & J_2 &= H_1 - H_2 = L_1 \sqrt{1 - e_1^2} \cos I_1 - L_2 \sqrt{1 - e_2^2} \cos I_2.\end{aligned}$$

Since the averaged disturbing function R depends on the nodes only through $\Delta\Omega = \Omega_1 - \Omega_2$ (Brouwer and Clemence 1961), the angle θ_1 is cyclic in the expression of R ; hence, its conjugate action J_1 is constant of motion.

In terms of canonical heliocentric elliptical elements, the components of the total angular momentum \vec{C} are

$$\begin{aligned}C_x &= \sum_{i=1}^2 L_i \sqrt{1 - e_i^2} \sin I_i \sin \Omega_i, \\ C_y &= \sum_{i=1}^2 L_i \sqrt{1 - e_i^2} \sin I_i \cos \Omega_i, \\ C_z &= \sum_{i=1}^2 L_i \sqrt{1 - e_i^2} \cos I_i.\end{aligned}$$

The direction of the constant total angular momentum defines a plane, orthogonal to \vec{C} in the space, which is an invariant of the problem (this plane is known as the Laplace plane). The choice of the Laplace plane as the reference plane of coordinates implies that $C_x = C_y = 0$ and $C_z = \|\vec{C}\| = \text{const.}$

If we assume that both planets turn around the central star in the same sense, we obtain from the condition $C_x = C_y = 0$ that the planetary eccentricities and inclinations are such that

$$G_1 \sin I_1 = G_2 \sin I_2. \quad (4)$$

The consequence of this condition is that, for $C_z > 0$, the variation of the inclinations of the planets is confined between zero and 90° , with a degeneracy of the problem at $I_i = 90^\circ$. The motions of the ascending nodes referred to the invariant plane are coupled in the following way:

$$\Omega_1 = \Omega_2 \pm 180^\circ.$$

The immediate consequence of this condition is that the problem is invariant under rotation of the angle $\Delta\Omega$ by 180° .

Based on the invariance of the direction of \vec{C} , we can partially reduce the system by one degree of freedom (Malige *et al.* 2002). In addition, using the invariance of the norm of the total angular

momentum, we can perform the reduction by one more degree of freedom. Indeed, the condition given by $\|\vec{C}\| = C_z$ constrains the action variables of the problem, in such a way that

$$\begin{aligned} J_1 &= H_1 + H_2 = C_z, \\ J_2 &= H_1 - H_2 = (G_1^2 - G_2^2)/C_z. \end{aligned} \quad (5)$$

Introducing the explicit dependence on C_z in the Hamiltonian (3), we perform the total reduction and obtain, as a result, a two-degrees-of-freedom model.

Instead of the total angular momentum C_z , the use of the Angular Momentum Deficit (AMD) is more appropriated. This quantity is defined as (Poincaré 1897, Laskar 2000)

$$\text{AMD} = L_1 + L_2 - C_z = \sum_{i=1}^2 L_i (1 - \sqrt{1 - e_i^2} \cos I_i).$$

and has a minimum value (zero) for circular co-planar orbits and increases with increasing eccentricities and inclinations.

In this work, we use both total and partial reductions to study the 3-D dynamics of the planetary system. In the first case, we choose a pair of independent action variables and the corresponding two angles. The other pair of actions can be easily obtained using Eqs. (5), for a given value of C_z . Here, we opt for two different pairs of the action variables: one is (G_1, G_2) (that is, e_1 and e_2) and other is (G_1, H_1) (that is, e_1 and I_1). In the case of partial reduction, the system has three degrees of freedom and the set of the variables used consists of the eccentricities of the planetary orbits and their mutual inclination. The individual inclinations of the planetary orbits are obtained using Eq. (4).

The model developed in this paper has been applied to the study of the topology of the phase space of the ν Andromedae planetary system (planets **C** and **D**). The results, presented and discussed in detail in the following sections, are in very good accordance with those obtained through direct numerical integrations of equations of motion. This is mainly due to principal advantage of the model: it has no restrictions about the magnitude of the planet eccentricities and inclinations. The main disadvantage of the semi-analytical model is related to high computational costs of the direct integrations of the canonical equations of motion. For this reason, the developed model was used to characterize the phase space of a dynamical system, through the calculation of the energy levels and the families of periodic orbits. The planetary paths were obtained through the direct numerical integrations of equations of motion.

3 Geometrical pictures of the 3-D secular dynamics

The interpretation of the results of numerical investigations becomes easier when preceded by the study of the main features of the semi-analytical model developed in the previous section. For this reason, in this section, we present the phase space topology of the Hamiltonian system given by Eq. (3) and analyze its relationship with planetary dynamics.

First, to visualize the dynamical features of the fully-reduced system, we introduce a representative plane of initial conditions. The initial conditions may be chosen in such a way that all possible configurations of the system are included, allowing us to obtain all possible regimes of motion of the system under study. The space of initial conditions of the two-degrees-of-freedom Hamiltonian

system given by Eqs. (2)–(3) is four-dimensional, but the problem can be reduced to the systematic study of a representative two-dimensional plane as follows.

We define the new angular variables of the problem. The first of them comes from the studies of the planar secular problem (MM2004): it is $\Delta\varpi = \varpi_1 - \varpi_2 = \omega_1 - \omega_2 + \Delta\Omega$, where ϖ_1 and ϖ_2 are the longitudes of the planetary pericenters and $\Delta\Omega = \pm 180^\circ$. We know that the angle $\Delta\varpi$ can either circulate or oscillate about 0 or 180° . In both cases, it goes through either 0 or 180° for all initial conditions. Hence, without loss of generality, the angular variable $\Delta\varpi$ can initially be fixed at 0 or 180° .

The choice of the second angular variable, as $2\omega_1$, is based on the particular property of the planetary disturbing function that requires the same parity of the indices preceding the planet arguments, ω_1 and ω_2 (Brumberg 1995). Indeed, using this property, we can re-write a generic periodic argument of the Hamiltonian function (3), $k\omega_1 + l\omega_2 + m\Delta\Omega$, as

$$\frac{k+l}{2}(2\omega_1) - l\Delta\varpi + (m+l)\Delta\Omega,$$

where $\Delta\Omega = \pm 180^\circ$ and k , l and m are integers which vary within the interval $(-\infty, +\infty)$. Our experimental studies have shown that the angular variable $2\omega_1$ can also either circulate or oscillate about 180° , which means that the argument of pericenter of the inner planet, ω_1 , either circulates or oscillates about $\pm 90^\circ$ (the sign depends on the chosen initial values of angle variables). In this case, it always goes through either 0 or $\pm 90^\circ$ for all initial conditions. Hence, the initial values of $2\omega_1$ can be also fixed at 0 or 180° .

Now, the dynamics of the twice-reduced Hamiltonian (3) can be represented on the plane of the initial values of the pair $(e_1 \cos \Delta\varpi, e_2 \cos 2\omega_1)$ (hereafter referred as to (e_1, e_2) representative plane), where e_1 and e_2 are the averaged planetary eccentricities. The information on the initial values of the angular variables is given by coordinate sign: positive (negative) values on x-axis correspond to $\Delta\varpi = 0$ (180°), while positive (negative) values on y-axis correspond to $2\omega_1 = 0$ (180°).

Figure 1 shows the level curves of the energy given by the averaged secular Hamiltonian (3) on the representative (e_1, e_2) -plane of initial eccentricities of the planets. The plane was constructed using $\text{AMD} = 3 \times 10^{-3}$, in units of the solar mass, astronomical unit and year. This value corresponds to the value of the Angular Momentum Deficit of the current *v* Andromedae system, assuming coplanar orbits. The thick curve shows the boundary of the energy manifold defined by the chosen value of AMD. Note the discontinuity in the phase space topology in the passage between the lower and upper half-planes.

The geometrical analysis of the secular behavior is based on the fact that the secular energy $\overline{H}_{\text{sec}}$ and AMD are both conserved along one solution. This is reflected on the representative plane of initial conditions in the following way: Independent of whether the motion of $\Delta\varpi$ and ω_1 is circulation or oscillation, an orbital path always passes through the conditions $\sin \Delta\varpi = 0$ ($\Delta\varpi = 0$ and/or 180°) and $\sin 2\omega_1 = 0$ ($\omega_1 = 0$ and/or 90°). This means that an individual quasi-periodic solution intersects the representative plane at four points and all points must belong to one energy level. Of these points, one point is the chosen initial condition, and the other three point are its counterparts. The exceptional cases are: 1) a stationary solution, which appears as fixed point on the plane; 2) periodic solutions, which have one of the angles fixed and, consequently, intersect the plane at only two points; and 3) orbits of chaotic motion, which, due to diffusion processes, intersect an energy level on the (e_1, e_2) -plane at an arbitrary number of points.

Fig. 1

The qualitative behavior of the angular variables, $\Delta\varpi$ and ω_1 , can be assessed from the geometrical analysis of the representative plane in Fig. 1. Concerning the behavior of the angle $\Delta\varpi$: if all intersections of an orbital path are located at the positive x -axis side of the (e_1, e_2) -plane, the angle $\Delta\varpi$ oscillates around zero. Conversely, if all points are located at the negative x -axis side of the plane, $\Delta\varpi$ oscillates around 180° . Finally, when the intersections are at the opposite half-planes with respect of x -axis, the orbits of both planet are circulating with respect of the angle $\Delta\varpi$.

In what concerns the behavior of the angle ω_1 , if all points of an orbital path are located at the negative y -axis side of the (e_1, e_2) -plane, the angle ω_1 oscillates around $\pm 90^\circ$. When the intersections are in the opposite half-planes with respect to the x -axis, the orbital paths are circulating with respect of ω_1 .

The level of the maximal secular energy, $\overline{H}_{\text{sec}} = -1.02370 \times 10^{-4}$, appears in Fig. 1 as a fixed point with coordinates $e_1 \cos \Delta\varpi = -0.33$ and $e_2 \cos 2\omega_1 = -0.02$, corresponding to $I_{\text{mut}} = 42^\circ.9$. This is a stationary solution of the secular Hamiltonian, which is characterized by constant eccentricities and inclinations. In the close vicinity of the stationary solution, the angles $\Delta\varpi$ and ω_1 (consequently, ω_2) are oscillating around 180° and $\pm 90^\circ$, respectively.

We also show in Fig. 1 six levels with decreasing energy denoted by letters from **a** to **f**. Several examples of intersections of planetary paths with the (e_1, e_2) -plane are shown by different symbols. The level **a** ($\overline{H}_{\text{sec}} = -1.02377 \times 10^{-4}$), close to the stationary solution, is located at the quadrant of the plane corresponding to conditions $\Delta\varpi = 2\omega_1 = 180^\circ$. The possible solutions in this case are oscillations of both angles $\Delta\varpi$ and ω_1 (and ω_2) around 180° and $\pm 90^\circ$, respectively. Four crosses along the level show the intersection of one solution with the representative plane.

With decreasing energy, the energy levels split into two unconnected branches: one is in the low-left quadrant, while the other is in the low-right quadrant. The level **b**, with $H_{\text{sec}} = -1.0247 \times 10^{-4}$, is an example; note that the initial conditions along this level are located far away from the origin of the plane. The location of this level on the lower half-plane indicates that all solutions have ω_1 oscillating around $\pm 90^\circ$. On the other hand, the secular angle $\Delta\varpi$ is allowed now to circulate or oscillate around 180° , depending on the initial conditions. One solution on this level, presented by four crosses, has the angle $\Delta\varpi$ in retrograde circulation. Initial conditions leading to solutions with $\Delta\varpi$ oscillating around 180° with a very small amplitude are shown by full circles. As we will see later, the passage from oscillation to circulation of $\Delta\varpi$ in this case is merely kinematical and there is no real separatrix between two modes of motion, which evolve continuously from one to another.

Along the level **c**, with $\overline{H}_{\text{sec}} = -1.0257 \times 10^{-4}$, most initial conditions are still characterized by the libration of ω_1 around $\pm 90^\circ$ and circulation of $\Delta\varpi$ (one example of this kind of motion is given by four crosses which belong to this level). The exceptions are solutions in the close vicinity of the origin of the plane, where the transition to the circulation mode of motion of ω_1 occurs. To better illustrate this feature, we show in Fig. 2 the surface of section and dynamic spectrum constructed on the energy level **c**. The phase space (top panel) is dominated by the regime of ω_1 -libration, with the fixed point at $e_1 = 0.29$, corresponding to $e_2 = 0.1$ and $I_{\text{mut}} = 41^\circ.8$. A separatrix between circulation and libration of ω_1 involves the origin of the plane in Fig. 2. A new regime of motion appears near the origin: this is a true secular resonance of the angle $\Delta\varpi$ librating around 180° . The dynamic spectrum in Fig. 2 *bottom* shows its structure with separatrix located at $e_1 \cos 2\omega_1 = -0.1$ ($e_2 = 0.246$ and $I_{\text{mut}} = 34^\circ.7$).

This new dynamical feature is accentuated along the energy level **d**, with $\overline{H}_{\text{sec}} = -1.027 \times 10^{-4}$. The level is now a continuous curve on the lower half-plane, with a new branch appearing on

Fig. 2

the upper half-plane, where $\omega_1 = 0^\circ$. This geometry is also characteristic for the levels **e**, with $\overline{H}_{\text{sec}} = -1.029 \times 10^{-4}$, and **f**, with $\overline{H}_{\text{sec}} = -1.038 \times 10^{-4}$, in Fig. 1. Along the energy level **d**, we have detected initial conditions leading to the solutions of three distinct regimes of motion, depending on the initial conditions. They are 1) a libration of ω_1 around $\pm 90^\circ$ and a circulation of $\Delta\varpi$ (shown by crosses); 2) a libration of $\Delta\varpi$ around 180° and a circulation of ω_1 (full circles); 3) a circulation of both angles (triangles). The regions of transition between domains of different regimes are characterized by chaotic motion; one solution of chaotic motion is represented by star symbols, which are randomly distributed along the energy level **d**. To access the type of motion of one solution requires an additional information, which we obtain by direct numerical integrations of the equations of motion and are presented in the next section.

As a final consideration, our numerical investigations have shown that the variables e_1 and e_2 , together with I_1 and I_2 , reach their maximal and minimal values at the conditions $\cos \Delta\varpi = \cos 2\omega_1 = 0$. This fact allows us to estimate the ranges of the eccentricity variation for both planets analyzing the geometrical picture presented in Fig. 1.

4 Topology and dynamical maps of the representative planes

In this section we present the results of investigations of the 3-D dynamics of the outer *v* Andromedae system obtained through the semi-analytical approach described above and numerical integrations of the exact equations of motion. The results are presented in the form of the topological and the dynamical maps calculated for $\text{AMD} = 3 \times 10^{-3}$.

To fully represent the secular dynamics, we have chosen two subspaces of initial conditions: one is the (e_1, e_2) -plane of initial eccentricities of the planets, introduced in the previous section, and other is the (e_1, I_1) -plane of initial eccentricity and inclination of the inner planet. In both cases, the initial values of the angular variables of the problem, $\Delta\varpi$ and $2\omega_1$, were fixed at either zero or 180° . The information on the initial values of the angular variables is given by the coordinate sign, as described in the previous section.

It is easy to show that both phase planes are equivalent: the solutions on one of these planes may be obtained from those on the other through Eqs. (5), for a given AMD. Nevertheless, we present two planes due to the fact that the (e_1, e_2) -plane is good to display the details in high planetary inclinations, while the low inclination behavior is confined to the very narrow vicinity of the borders. At variance, the (e_1, I_1) -plane shows clearly the details of the low inclination dynamics.

Figure 3 shows the topology (*left*) and dynamical maps (*right*) on the (e_1, e_2) -plane (*top*) and (e_1, I_1) -plane (*bottom*). The location of the coplanar *v* Andromedae system (planets **C** and **D**) is shown by star symbol on all panels. The levels curves of the energy are plotted with solid lines on the topological maps. The mutual inclination between the orbital planes is given by hatched lines on the (e_1, e_2) -plane. On the (e_1, I_1) -plane the hatched curves show the levels of $e_2 = \text{const.}$ For $\text{AMD} = 3 \times 10^{-3}$, the system reaches the maximal value of the mutual inclination at $47^\circ.4$, when $e_1 = e_2 = 0$, while the maximal value of the eccentricity of the outer planet is 0.365, at $e_1 = I_1 = 0$.

The main families of the periodic orbits are plotted on the topological maps in Fig. 3 (*left*) by thick curves: The red curves are associated to solutions of the Hamiltonian (3) with the oscillating angle $\Delta\varpi$, while the blue curves to solutions with the librating ω_1 . Note that the oscillation of the secular angle $\Delta\varpi$ does not imply necessary the resonant behavior, but may be just a kinematical continuation of the circulation regime of motion (see MM2004). Moreover, the stability of the periodic solutions should be studied using appropriate techniques, but this is beyond the scope

Fig. 3

of the present work. In this work, the character of motion on each orbit is assessed through the identification of the regimes of motion of the system in the whole phase space by pure numerical methods. Even thus, the calculation of the periodic solutions provides an important information about a dynamical system, without time-expensive numerical integrations. It is worth mentioning that, with except of the oscillation solutions, these families present loci (stable and unstable) of the secular resonances in the phase space of the Andromedae system and are in very good agreement with the location of the secular resonances obtained by numerical integrations (see description of the dynamical maps below).

In the construction of the dynamical maps, a grid of 72×79 initial conditions was defined on the (e_1, e_2) -plane of planet eccentricities, with steps $\Delta e_1 = 0.02$ and $\Delta e_2 = 0.01$. The initial inclinations were obtained from Eqs. (5), for $\text{AMD} = 3 \times 10^{-3}$. The angular variables used were: from the set I in the right-top quadrant, the set II in the left-top quadrant, the set III in the left-bottom quadrant and the set IV in the right-bottom quadrant of the (e_1, e_2) -plane (see the Appendix). On the (e_1, I_1) -plane, a grid of 72×81 initial eccentricity and inclination of the inner planet was defined with steps $\Delta e_1 = 0.02$ and $\Delta I_1 = 1^\circ$. The initial eccentricity and inclination of the outer planet were obtained using Eqs. (5). The distribution of the initial angular orbital elements of the planets is identical to the previous case.

The shading scale used on the dynamical maps in Fig. 3 (*right*) is related to the degree of stochasticity of the solutions: the lighter regions on the dynamical maps correspond to initial conditions of regular motion, darker tones indicate increasingly chaotic motion. The hatched zones are regions of forbidden motion, where no solutions of the Hamiltonian system (3) exist for $\text{AMD} = 3 \times 10^{-3}$. The limit of the domains of allowed and forbidden motion can be calculated using Eqs. (5): with conditions $I_1 = I_2 = 0$ on the (e_1, e_2) -plane and $e_2 = I_2 = 0$ on the (e_1, I_1) -plane.

The analysis of the structure of the dynamical maps on the representative planes reveals interesting topological properties and reflect important features of the 3-D secular dynamics in the region of the ν Andromedae planetary system. The (e_1, e_2) - and (e_1, I_1) -planes are dominated by a gray background of regular secular motion of the system. The narrow strips in white coincide with the location of the periodic solutions of the secular system. The domains of chaotic motion appear as black regions in Fig. 3 (*right*): they are associated with separatrices of different regimes of secular motion.

The careful analysis of the results of the numerical simulations, always accompanied by the study of the geometry of the energy levels and periodic solutions, allowed us to identify various different regimes of motion of the system. Their domains are marked by **1–4** on the dynamical maps in Fig. 3 (*right*). The domains **1** are regions of motion characterized by the coupled variation of the eccentricity and inclination of the inner planet and the libration of the angle ω_1 around $\pm 90^\circ$. They are located on the lower half-planes at high mutual inclination (above 35°). The white strips follow the location of the periodic resonant solution in these regions. This regime of motion is often referred to as Kozai resonance in the literature. In this work, we designate this resonance as e - I coupling, or Lidov resonance, to pay homage to the Russian scientist, who first discovered this dynamical phenomenon (Lidov 1961). The stationary solution of the secular Hamiltonian (3), together with the paths of energy levels from **a** to **c** shown in Fig. 1, belong to the domains of this resonance. The typical behavior of the secular angle $\Delta\varpi$ inside the Lidov resonance is a retrograde circulation or oscillation around 180° , the difference being merely kinematical.

The domains of the Lidov resonance are delimited in the phase space by the regions of strong chaotic motion, which appear as black zones on dynamical maps in Fig. 3 (*right*). In their close

vicinity, at lower inclinations, a new resonant regime of motion appears; its domains are labeled by **2** in Fig. 3. This resonance is characterized by the libration of the secular angle $\Delta\varpi$ around 180° and the prograde circulation of both angles ω_1 and ω_2 . The family of the stable periodic solution of this resonance can be observed as the narrow white strips inside the domains **2**.

The regime of motion in the region **2** is better illustrated on a surface of section. In Fig. 4, we show the surface of section and dynamic spectrum constructed along the energy level $\overline{H}_{\text{sec}} = -1.033 \times 10^{-4}$. The dominating regime of motion at this energy is the secular resonance of $\Delta\varpi$ described above, with the stable fixed point at $e_1 \cos \Delta\varpi = -0.385$ and $e_2 \cos 2\omega_1 = -0.187$, which correspond to $I_{\text{mut}} = 32^\circ.7$. The unstable fixed point of this resonance is located at $e_1 \cos \Delta\varpi = 0.433$ and $e_2 \cos 2\omega_1 = -0.147$, at the same mutual inclination.

We can see in Fig. 4 that the separatrix involving the secular resonance divides the whole domain of motion into the inner zone, close to the origin, and the outer zone. The inner region shows complex dynamical structure which is characteristic of the presence of secondary resonances. The dynamic spectrum of the solutions with initial conditions $e_1 \sin \Delta\varpi = 0$ (Fig. 4 *bottom*) reveals the existence of islands of regular motion inside the sea of chaos in this region. The behavior of the secular angles inside the inner region is a circulation: retrograde for $\Delta\varpi$ and prograde for ω_1 and ω_2 . The domains of this regime of motion are marked by label **3** on the dynamical maps in Fig. 3.

In the outer region in Fig. 4, the circulation of $\Delta\varpi$ inverts its direction. This change in the direction of motion of the secular angle $\Delta\varpi$ is a typical feature of the secular resonance. The domains of this regime of motion, characterized now by prograde circulation of all secular angles, $\Delta\varpi$, ω_1 and ω_2 , are shown by label **4** in Fig. 3. This regime of motion extends to inclinations close to 0 and is known from the study of dynamics of the planar planetary model (MM2004). For some initial conditions, the angle $\Delta\varpi$ oscillates around 0 or 180° ; the regions of oscillation of $\Delta\varpi$ in the domains **4** are seen as the white strips on the dynamical maps in Fig. 3. It should be emphasized that the difference between circulation and oscillation of $\Delta\varpi$ in this region is merely kinematical and there are no true separatrices between two modes of motion (MM2004). Thus, the 3-D dynamics of the system is nearly similar to that with coplanar orbits, even for mutual inclinations as large as 30° (Lee and Peale 2003).

The results on the possible regimes of motion of the outer *v* Andromedae system are summarized in Table I. In addition, it is interesting to comment some features which can be clearly observed inside the domains **4** in Fig. 3. As shown above, the secular planetary motion in these regions is regular, but darker tones, indicating increasingly chaotic motion, can be also seen in this region. The only explanation for this feature is due to an effect of the proximity of the system to mean-motion resonances of high order in these regions. Of course, the secular model developed in this work can not account for the effect of the mean-motion resonances, which will be studied through purely numerical techniques in the Section 7.

5 Dependence on the Total Angular Momentum Deficit

For small values of AMD, the dynamics of the system is very similar to that of the planar case. This is due to the fact that the values of the mutual inclination between the planetary orbits, allowed from Eqs.(5), in this case, are small. In Fig. 5, we present the topological picture of the phase space of the system with $\text{AMD} = 1 \times 10^{-3}$, plotting the energy levels on the (e_1, e_2) - and (e_1, I_1) -planes. The maximal value of the mutual inclination between orbital planes is 27° . The typical signatures of the high inclination behavior, such as the existence of stationary solutions and

Fig. 4

Table I

bifurcations of the energy levels, shown in the previous sections, are not observed in Fig. 5. Only periodic solutions corresponding to the secular angle $\Delta\varpi$ exist. This curve indicates the location of the domains of oscillation (about 0 and 180°) of $\Delta\varpi$, which is a kinematical continuation of the prograde circulation regime.

At variance, for the large values of the Angular Momentum Deficit, the domain of possible motion of the system is extended to very high eccentricities and inclinations. Figure 6 shows the topology (*left*) and dynamical maps (*right*) on the (e_1, e_2) -plane (*top*) and (e_1, I_1) -plane (*bottom*), constructed for $\text{AMD} = 8 \times 10^{-3}$. The notations used in this figure are analogous to those used in Fig. 3. The system reaches the maximal value of the mutual inclination at 79°.7, when $e_1 = e_2 = 0$; the maximal value of the eccentricity of the outer planet is 0.58, when $e_1 = I_1 = 0$. The location of a fixed point (stationary solution) is at $e_1 \cos \Delta\varpi = -0.81$ and $e_2 \cos 2\omega_1 = -0.1$, which correspond to $I_{\text{mut}} = 60^\circ.9$.

The geometry of the representative planes is similar to that obtained for $\text{AMD} = 3 \times 10^{-3}$. A new topological structure appears in Fig. 6 *left bottom*, in the low inclination region along the negative x-axis. This is an artifact of the model that appears in domains of the crossing orbits and disappears in the direct numerical integration tests.

Our previous studies of the planar problem (MM2004) have shown that the large values of the Angular Momentum Deficit are characterized by the presence of a secular resonance with the angle $\Delta\varpi$ librating around 0. Indeed, the domain of this resonance, denoted with the label **5**, is clearly seen on the dynamical map of the (e_1, I_1) -plane in Fig. 6 *right bottom*; on the (e_1, e_2) -plane, this regime of motion occupies a narrow domain near the border.

The high inclination regimes of motion described above (regimes **1** and **2**) are also present in Fig. 6. The domains of the Lidov resonance, shown by **1**, are dominating on the lower half-planes. The location of the periodic orbits of this resonance is in good agreement with that calculated from our 3-D model (blue curves on the topological maps). On the upper half-planes, we can observe the existence of the high inclination secular resonances with respect of $\Delta\varpi$: one is at positive e_1 -domain, where $\Delta\varpi$ librates around 0, and other is at negative e_1 -domain, where $\Delta\varpi$ librates around 180°.

6 Dependence on the mutual inclinations

In the previous sections, the analysis of the 3-D dynamics of the *v* Andromedae system was done with a system reduced to 2 degrees of freedom, whose evolution is constrained by a fixed value of the Angular Momentum Deficit. In this section, we consider the system only partially reduced to 3 degrees of freedom, where the direction of the angular momentum is taken into account, but not its modulus. In this case, we vary three orbital parameters of the problem; they are chosen as both planetary eccentricities and the mutual inclination of the planetary orbits. The study is done by means of dynamical maps and characteristic curves.

Figures 7 and 8 show the dynamical maps on the (e_1, e_2) -plane, obtained for three different values of the initial mutual inclination, namely 5°, 15° and 45°. In the construction of the maps, a grid of 100×61 initial eccentricities was defined on the (e_1, e_2) -plane. The angular variables used were: the set III, in the left-hand side of the panels, and the set IV, in the right-hand side of the (e_1, e_2) -plane (see the Appendix).

For $I_{\text{mut}} = 5^\circ$ and 15° , the domains of regular motion are characterized by either oscillation or circulation of $\Delta\varpi$. The light regions of the phase space correspond to oscillation of $\Delta\varpi$: either

Fig. 5

Fig. 6

Fig. 7

around 0, on the e_1 -positive half-plane, or around 180° , on the e_1 -negative half-plane. The regions in gray code are regions of regular orbits with circulating $\Delta\varpi$. Finally, the regions of highly nonharmonic and chaotic motion (dark zones) are domains of initial conditions leading to close approaches of two planets.

The hatched regions are regions of large-scale instability followed by disruption of the system within the time-interval of 530,000 years. The location of the current ν Andromedae system is shown by a star on both panels in Fig. 7. For the presently known best-fit planetary parameters, this system is within the domain where $\Delta\varpi$ oscillates around zero, as has been noted in previous studies (Malhotra 2002, Chiang & Murray 2002). The effect of the mean-motion resonances of high orders may be noted as a slightly nonharmonic feature in the close proximity of the system on both panels in Fig. 7.

Fig. 8

The domain of the true secular resonance reported by MM2004 is seen at the high eccentricity region of regular motion near the right border. The resonant orbits are protected from close approaches by coupled variation of the planet eccentricities and libration of $\Delta\varpi$. It is interesting to observe that the orbit of the inner planet inside this resonance can reach eccentricities as high as 0.95, but the system of two planets continues to be stable (at least, over the time-interval of 530,000 years).

The differences between the dynamical features revealed by two planes in Fig. 7 (obtained for $I_{\text{mut}} = 5^\circ$ and 15°) are negligible. We conclude that the dynamics of the 3-D system varies slowly in the low inclination region and is similar to the dynamics of the planar system studied in detail in (MM2004). This conclusion is in agreement with the results obtained by Lee and Peale (2003).

Significant changes in the dynamics of the system take place for the initial mutual inclinations larger than 30° . The dynamical map obtained with $I_{\text{mut}} = 45^\circ$ is shown in Fig. 8. The Lidov resonance is now dominating over the whole domain of regular motion. The analytically calculated characteristic curves of this resonance (in blue color) are in very good agreement with the results of numerical calculations (white strips).

The secular angle $\Delta\varpi$ circulates for almost all initial conditions, but, depending on the initial conditions, there are also oscillations around 180° in the low e_2 region. The red curves obtained from our model show the location of the oscillating $\Delta\varpi$. In the very high eccentricity region in Fig. 8, the narrow domain of the true secular resonance exists: it is characterized by libration of the angle $\Delta\varpi$ around 180° .

Finally, domains of chaotic motion appear in Fig. 8 as inclined black stripes of variable width; they are associated with the effects of the mean-motion resonances in the neighborhood of the system.

7 Mean-motion resonances in the neighborhood of the ν Andromedae Planetary System

On the dynamical maps discussed above, a peculiar feature, which could not be explained by the secular behavior of the system, is always present: the existence of slightly chaotic regions inside the low-inclination domains of the regime 4 in Fig. 3. Careful analysis of the output of numerical integrations allowed us to identify the origin of this phenomenon as an effect of mean-motion resonances present in the neighborhood of the system under study. Of course, the analytical model of secular motion can not predict this feature, and it was studied with purely numerical techniques.

The neighborhood of the ν Andromedae system was investigated with a dynamical map method. The initial conditions of the simulations were uniformly distributed on the (a_2, e_2) -plane of the semi-major axis and eccentricity of the outer planet, within the domains $2.4 \text{ AU} \leq a_2 \leq 2.7 \text{ AU}$ ($\Delta a_2 = 0.005 \text{ AU}$) and $0 \leq e_2 \leq 0.6$ ($\Delta e_2 = 0.01$), respectively. The initial inclination of the outer planet was fixed at 1° . The semi-major axis and eccentricity of the inner planet were fixed at their current values. We have chosen the set I of initial values of angular variables, and, to have the motion referenced to the invariant plane, we have calculated the inclination of the inner planet using Eq. (4).

Figure 9 shows the dynamical map obtained for the neighborhood of the outer planet **D**. Once again, the shading scale was used to distinguish between the regions of regular and chaotic motion. The domains of chaotic motion, which appear in Fig. 9, are associated with mean motion resonances. We note the dominating presence of the 5:1 resonance: this is the resonance of the lowest order (4) in this region. Weaker resonances of higher orders appear in Fig. 9 as black stripes of variable width: they are the 11:2, 16:3 and 21:4 resonances of orders 9, 13 and 17, respectively. The ν Andromedae system is close to the 16:3 resonance. Despite the very high order of this resonance, its effect can still be seen on dynamical maps.

Fig. 9

8 Conclusions

We have developed a new semi-analytical approach that is an extension of the secular model presented in (MM2004) and describes the three-dimensional dynamics of the planetary system. The used technique is the numerical averaging over short-periods of the mutual interaction of the two planets. We emphasize that, in the present work, we do not use expansions of the disturbing function in power series of the planetary eccentricities and inclinations nor in Fourier series of the angular variables, such as done in many previous analyzes (e.g., Brouwer and Clemence 1961). This means that the secular motion of the planets is described very precisely, without any restriction about the magnitude of their eccentricities and inclinations, the mutual distance and the masses ratio. The only condition for the applicability of the model is that the system must be located outside a strong mean-motion resonance.

Due to the invariance of the total angular momentum, the 3-D secular problem is reducible to a two-of-degree-of-freedom dynamical system (total or Jacobi reduction). To investigate the dynamics for different values of AMD, we use also a partial reduction to a three-degrees-of-freedom system, taking into account only the invariance of the angular momentum direction, not its modulus. We present geometrical pictures of the secular phase space of the two-planet system in terms of eccentricities and inclinations. Owing to the symmetries in the secular Hamiltonian, the phase space structure can be visualized in representative planes of initial conditions, with initial angular elements, $\Delta\varpi$ and $2\omega_1$, fixed at either 0 or 180° .

The analysis of the topology of the phase space of the Hamiltonian system given by Eq. (3) allow us to estimate the range of the eccentricity/inclination variations without time-expensive numerical integrations of the equations of motion. The qualitative study was supplemented by direct numerical integrations over a wide range of initial conditions and the interpretation of the results was always founded on both analytical approaches.

We applied this analysis to the specific case of the system of two outer planets, **C** and **D**, of ν Andromedae. The topology of the phase space of the system was investigated by means of several techniques, nominally: energy levels construction, periodic orbits and characteristic curves plotting,

surfaces of section, dynamic spectra and dynamical maps.

We summarize the following important features of the 3-D dynamics of the ν Andromedae system.

1. The low-to-moderate eccentricity and mutual inclination regime of motion (domain **4** with $e_1 < 0.6$ and $I_{\text{mut}} < 30^\circ$): this regime is similar to planar solutions, where all secular angles are in regular direct circulation. The secular behavior of the ν Andromedae system is generally stable; instabilities occur only in the vicinity of the high-order 16:3 mean-motion resonance. The systems always exhibit two main regimes of motion, characterized by circulation of $\Delta\varpi$ or its oscillation around 0 or 180° . There are no real separatrices between two modes of motion, which evolve continuously from one to another; the only differences are merely kinematical.

2. The high eccentricity and low-to-moderate inclination regime (domain **5** with $e_1 > 0.6$ and $I_{\text{mut}} < 30^\circ$) is characterized by large-scale instabilities, due to close approaches of the planets, followed by disruption of the system within a few thousands of years. The only survival solutions in this region are those from the nonlinear secular resonance zone bounded by a zero-frequency separatrix. The secular angle $\Delta\varpi$ librates around 0 and the variation of e_1 and e_2 is strongly coupled. This feature of the secular dynamics of two-planet systems has been previously studied in (MM2004).

3. The high inclination regime (domains **1** – **3** with $I_{\text{mut}} > 30^\circ$): complex dynamical behavior with the presence of several regimes of resonant motion. The dominating behavior is the e – I coupling, or Lidov resonance, characterized by the coupled variation of the eccentricity and inclination of the inner planet and the libration of the angle ω_1 around $\pm 90^\circ$. At variance with the analogous phenomenon in restricted problems, the variation of the planet inclinations and eccentricities is constrained by the total angular momentum conservation. Hence, the large eccentricity/inclination excursions induced by the Lidov resonance can not occur in the planetary problem. A regime of motion with $\Delta\varpi$ in the secular resonance also exists in the high-inclination region. In this case, the secular angle $\Delta\varpi$ librates either around 0 or 180° .

9 Appendix. Numerical methods

In this section we describe the main numerical techniques used in the study of the dynamics of the ν Andromedae system.

Energy levels calculation. The topology of the phase space of the Hamiltonian system can be studied by plotting the energy level curves on the representative planes of initial conditions. For this purpose, the equation $\overline{H}_{\text{sec}} - H^* = 0$ is solved numerically, for a given value of the energy H^* , using a numerical procedure for root finding. The secular Hamiltonian function $\overline{H}_{\text{sec}}$ is given by Eq. (3). Applying the total reduction, we choose a pair of action variables and the other pair is obtained through Eqs. (5). The pair of independent variables may be, for instance, the pair (G_1, G_2) (equivalently, e_1, e_2). In this case, for given H^* and AMD, e_1 can be easily obtained as a function of e_2 . Varying H^* , we calculate a family of the energy levels and plot it on the representative (e_1, e_2) -plane.

Calculation of the characteristic curves and the families of the periodic orbits. The characteristic curves of the Hamiltonian (3) give information on the location of the zero precession

rates of the angular variables. They are obtained through the following conditions:

$$\dot{\omega}_1 = \frac{\partial \overline{H}_{\text{sec}}}{\partial G_1} = 0, \quad \dot{\omega}_2 = \frac{\partial \overline{H}_{\text{sec}}}{\partial G_2} = 0. \quad (6)$$

By definition, the difference of the planet periastron longitudes is $\Delta\varpi = \omega_1 - \omega_2 + \Delta\Omega$, where $\Delta\Omega = 180^\circ$. Consequently, we obtain the condition $\Delta\dot{\varpi} = \dot{\omega}_1 - \dot{\omega}_2 = 0$ for the zero precession rate of the secular angle $\Delta\varpi$. The derivatives can be computed for any given point of the phase space using the second-order differencing scheme (Press *et al.* 1986).

It should be emphasized that, for the system with two or more degrees of freedom, the conditions (6) do not define the families of periodic orbits. In this work, we present the curves characterized by $\dot{\omega}_1 = 0$ and $\Delta\dot{\varpi} = 0$ just as an indication of the domains of possible libration of the corresponding angles.

According to the definition, a time evolution of an angle ϕ is periodic, with period T , if

$$\phi(t) = \phi(t + T),$$

for *all* values of t . A two-degrees-of-freedom dynamical system is characterized by two fundamental frequencies, consequently, a general (quasi-periodic) solution of this system is a composition of two independent modes of motion. In this case, the condition of periodicity will be satisfied when the amplitude of one of two modes tends to zero. Thus, the precise location of the periodic trajectories can be calculated numerically from the position of the fixed points on the surfaces of section.

Numerical integration. In order to obtain planetary paths, the exact equations of planetary motion were numerically integrated in the framework of the three-body general problem. The accurate RA15 integrator (Everhart 1985) was used. To compare the results of numerical investigations with the results given by the developed model, we use the canonical heliocentric orbital elements of the planets, instead the usual osculating heliocentric elements. The transformation between these two sets can be found in detail in (Ferraz-Mello *et al.* 2004).

The initial conditions of the pair of the independent variables used in the simulations were uniformly distributed in the space of canonical orbital elements. The angular orbital elements of the planets, ω_i and M_i (arguments of pericenter and mean anomalies of the inner ($i = 1$) and outer ($i = 2$) planets) were fixed at the following four sets:

Set I ($\cos \Delta\varpi = 1$ and $\cos 2\omega_1 = -1$):

$$\begin{aligned} \omega_1 &= -90^\circ & M_1 &= 0^\circ \\ \omega_2 &= 90^\circ & M_2 &= 0^\circ \end{aligned}$$

Set II ($\cos \Delta\varpi = -1$ and $\cos 2\omega_1 = -1$):

$$\begin{aligned} \omega_1 &= 90^\circ & M_1 &= 180^\circ \\ \omega_2 &= 90^\circ & M_2 &= 0^\circ \end{aligned}$$

Set III ($\cos \Delta\varpi = 1$ and $\cos 2\omega_1 = 1$):

$$\begin{aligned} \omega_1 &= -180^\circ & M_1 &= 0^\circ \\ \omega_2 &= 0^\circ & M_2 &= 0^\circ \end{aligned}$$

Set IV ($\cos \Delta\varpi = -1$ and $\cos 2\omega_1 = 1$):

$$\begin{aligned}\omega_1 &= 0^\circ & M_1 &= 180^\circ \\ \omega_2 &= 0^\circ & M_2 &= 0^\circ\end{aligned}$$

For all sets, the initial value of $\Delta\Omega = \Omega_1 - \Omega_2$ was fixed at 180° . For a given value of Angular Momentum Deficit, the initial values of the other pair of variables can be obtained from Eqs. (5). This condition guarantees that the used reference frame is invariant.

In order to apply the developed model to the planets **C** and **D** of the v Andromedae system, we adopt the following parameters: the masses $m_0 = 1.3M_{\text{Sun}}$, $m_1 = 1.83M_{\text{Jup}}$ and $m_2 = 3.97M_{\text{Jup}}$, for the central star, inner planet C and outer planet D, respectively; the semi-major axes $a_1 = 0.83$ AU and $a_2 = 2.56$ AU; and the planet eccentricities $e_1 = 0.25$ and $e_2 = 0.34$ at $\Delta\varpi = 0$ and $2\omega_1 = 0$. The masses correspond to the planetary orbits observed edge-on, so $\sin i = 1$ for each planet, where i is the orbital inclination to the plane of the sky. The units adopted in this work are the solar mass, astronomical unit and year.

To remove the short-period oscillations (those of the order of the planetary orbital periods), a low-pass filtering procedure was implemented on-line with the numerical integration as described in detail by Michtchenko and Ferraz-Mello (1995). The numerical integrations were performed over a time interval of 524,544 years, which was large enough to allow an accurate and efficient averaging of the long-period effects, and also to detect the occurrence of secular resonances.

Dynamical maps. The orbital paths of the planets obtained through direct numerical integrations were Fourier-transformed using the standard FFT algorithm. The information contained in the power spectra of the orbital elements was used in the construction of dynamical maps (see Michtchenko *et al.* 2002).

The mapped quantity is the spectral number N defined as the number of peaks in the power spectrum of one calculated planetary path above an arbitrarily defined "noise". In this work, we consider as "noise" those peaks with amplitudes smaller than 5% of the amplitude of the largest peak. The spectral number N is used to qualify the chaoticity of planetary motion in the following way: small values of N correspond to regular motion, while the large values indicate the onset of chaos.

Once the spectral numbers N are determined for all the initial conditions on the grid, we plot them on the representative plane using a shading scale. The calculated values of N , in the range from 1 to 80, are coded by a gray level scale that varied from white ($N = 1$) to black ($N = 80$). Since large values of N indicate the onset of chaos, the shading scale is related to the degree of stochasticity of the initial conditions: lighter regions on the dynamical maps correspond to regular motion, darker tones indicate increasingly chaotic motion.

Surfaces of section and Dynamic power spectra. The structure of the phase space of the two-degrees-of-freedom system may be studied using the standard technique of the construction of surfaces of section.

Two sections have been chosen for presentation in this work: The first is a section by the plane $\sin 2\omega_1 = 0$ and its coordinates are $e_1 \cos \Delta\varpi$ and $e_1 \sin \Delta\varpi$. The second is a section by the plane $\sin \Delta\varpi = 0$ and its coordinates are $e_1 \cos 2\omega_1$ and $e_1 \sin 2\omega_1$.

It should be emphasized that, in the construction of the surfaces of section, we have used as input the planetary solutions obtained by direct numerical calculations (the application of on-line

filtering procedure is crucial in this task). For this reason, the erratic scatter of points due to the loss of numerical accuracy can be sometimes observed.

The dynamic power spectra is a technique which is complementary to the surfaces of section, which is very efficient to identify such phenomena as bifurcation and chaoticity. A dynamic spectrum presents the evolution of the main oscillation modes of the planetary motion as a function of one dynamical parameter. Over the domains of regular motion, the proper frequencies vary continuously when the parameter is gradually varied. When the region of chaotic motion is approached, the frequency evolution shows a discontinuity, characterized by the erratic scatter of values.

Acknowledgments

We thank Dr. Renu Malhotra for suggesting the problem and the analysis method. This work has been supported by the Brazilian National Research Council - CNPq, as well as the São Paulo State Science Foundation - FAPESP. The authors gratefully acknowledge the support of the Computation Center of the University of São Paulo (LCCA-USP) for the use of their facilities.

REFERENCES

- Brouwer, D., and G.M. Clemence 1961. "Methods of Celestial Mechanics". Academic Press Inc., New York.
- Brumberg, V. A. 1995. "Analytical Techniques of Celestial Mechanics". Springer, Berlin.
- Chiang, E.I., D. Fischer, and E. Thommes 2002. Excitation of Orbital Eccentricities of Extrasolar Planets by Repeated Resonance Crossings. *ApJ* **564**, L105-L109.
- Everhart, E., 1985. An efficient integrator that uses Gauss-Radau spacings. *Proceedings of IAU Colloq. 83* 115, 185-202.
- Ferraz-Mello, S., T.A. Michtchenko, and C. Beaugé 2004. Regular motions in extra-solar planetary systems. NATO ASI Series C: Mathematical and Physical Sciences. , to be published in "Chaotic Worlds: From Order to Disorder in Gravitational N-Body Systems" (B.A.Steves, ed.), Kluwer Acad. Publ. (in press).
- Ferraz-Mello, S., T.A. Michtchenko, and C. Beaugé 2005. The Orbits of the Extrasolar Planets HD 82943 c and b. *ApJ* **621**, 473-481.
- Jacobi, C.G.J. 1842. "Sur l'élimination des noeuds dans le problème des trois corps". *Astronomische Nachrichten*, Bd XX , 81-102.
- Konacki, M., and A. Wolszczan 2003. Masses and orbital inclinations of planets in the PSR B1257+12 system. *ApJ* **591**, L147-L150.
- Laplace, P.S. 1799. "Mécanique Céleste". English translation by N. Bowditch, Chelsea Pub. Comp. Edition, N.Y., 1966.
- Laskar, J. 2000. On the Spacing of Planetary Systems. *Physical Review Letters* **84**, 3240-3243.
- Lee, M.H., and S.J. Peale 2003. Secular Evolution of Hierarchical Planetary Systems. *ApJ* **592**, 1201-1216.

- Lidov, R. 1961. Analiz evolucii orbit iskustvennich sputnikov. *Problemi dvigenia iskustvennich nebesnich tel*, Izd. Akademii Nauk SSSR, Moscow (1963), 119-134.
- Malhotra, R. 2002. A Dynamical Mechanism for Establishing Apsidal Resonance. *ApJ* **575**, L33-L36.
- Malige, F., P. Robutel, and J. Laskar. 2002. Partial Reduction in the N-Body Planetary Problem using the Angular Momentum Integral. *Celest. Mech. Dynam. Astron.* **84**, 283-316.
- Michtchenko, T.A., and S. Ferraz-Mello 1995. Comparative study of the asteroidal motion in the 3:2 and 2:1 resonances with Jupiter. I. Planar model. *Astronomy and Astrophysics* **303**, 945-963.
- Michtchenko, T.A., D. Lazzaro, S. Ferraz-Mello, and F. Roig 2002. Origin of the basaltic asteroid 1459 Magnya: A dynamical and mineralogical study of the outer main belt. *Icarus* **158**, 343-359.
- Poincaré, H. 1897. Sur une forme nouvelle des équations du problème des trois corps. *Bull.Astron.* **14**, 53-67.
- Press, W.H., Flannery, B.P., Teukolsky, S.A, and Vetterling, W.T. 1986. Numerical Recipes. Cambridge University Press.
- Veras, D., and Armitage, P.J. 2004. The dynamics of two massive planets on inclined orbits. *Icarus* **172**, 349-371.

Table 1: The main regimes of motion of the ν Andromedae system. The behavior of the angles ω_1 and $\Delta\varpi$ is identified by symbols: L – libration, CP and CR – prograde and retrograde circulation, respectively, O – oscillation.

Label	ω_1	$\Delta\varpi$	I_{mut}
1	L ($\pm 90^\circ$)	O (180°) /CR	$> 35^\circ$
2	CP	L (180°)	$\sim 30^\circ$
3	CP	CR	$\sim 30^\circ$
4	CP	CP	$< 30^\circ$

Figure Captions

Figure 1. Schematic details of the phase space on the representative (e_1, e_2) -plane of initial conditions obtained for $\text{AMD} = 3 \times 10^{-3}$. Six levels, from **a** to **f**, are at the decreasing energy. The fixed point is a stationary solution of the Hamiltonian (3). The intersections of some numerically calculated orbits with the plane are shown by : 1) crosses – the angle ω_1 in libration around $\pm 90^\circ$ and $\Delta\varpi$ in circulation; 2) full circles – the angle ω_1 in libration around $\pm 90^\circ$ and $\Delta\varpi$ oscillating around $\pm 180^\circ$; 3) triangles – the angles ω_1 and $\Delta\varpi$ in regular circulation; 4) stars – the angle ω_1 and $\Delta\varpi$ in chaotic circulation.

Figure 2. (*Top*:) Surfaces of section on the $(e_1 \cos 2\omega_1 \times e_1 \sin 2\omega_1)$ – plane, obtained at condition $\sin \Delta\varpi = 0$ and $\text{AMD} = 3 \times 10^{-3}$. (*Bottom*:) Dynamic spectrum corresponding to the solutions shown on the graph of surfaces of sections.

Figure 3. *Left*: Energy levels of the secular Hamiltonian given by Eq. (3) on the (e_1, e_2) -plane (*top*) and (e_1, I_1) -plane (*bottom*), for $\text{AMD} = 3 \times 10^{-3}$. The signs + or –, preceding the variable $e_1 \cos \Delta\varpi$ ($e_2 \cos 2\omega_1$ and $I_1 \cos 2\omega_1$), indicate that the initial values of $\Delta\varpi$ ($2\omega_1$) are zero or 180° , respectively. Periodic solutions of the secular Hamiltonian, corresponding to the oscillating $\Delta\varpi$ and librating ω_1 are shown by red and blue lines, respectively. The location of the v Andromedae system indicated by a star symbol. *Right*: Dynamical maps of the representative planes. The domains of different regimes of motion are: **1** – the Lidov resonance, where the angle ω_1 in libration around $\pm 90^\circ$ and $\Delta\varpi$ in retrograde circulation; **2** – the secular resonance, where the angle $\Delta\varpi$ in libration around 180° and ω_1 in circulation; **3** – the angles ω_1 and $\Delta\varpi$ in direct and retrograde circulation, respectively; **4** – all angles in direct circulation. The domains, where planetary collisions occur within 0.5 Myr, are hatched.

Figure 4. Same as in Fig. 2, but on the $(e_1 \cos \Delta\varpi \times e_1 \sin \Delta\varpi)$ -plane, obtained at condition $\sin \omega_1 = 0$.

Figure 5. Same as in Fig. 3 (*left column*), but for $\text{AMD} = 1 \times 10^{-3}$. The only periodic solutions of the secular Hamiltonian correspond to the oscillating $\Delta\varpi$.

Figure 6. Same as in Fig. 3, but for $\text{AMD} = 8 \times 10^{-3}$. The domain of the secular resonance, where the angle $\Delta\varpi$ in libration around 0° and ω_1 in circulation, are marked by **5**.

Figure 7. Dynamical maps of the (e_1, e_2) representative planes obtained for $I_{\text{mut}} = 5^\circ$ (*top*) and $I_{\text{mut}} = 15^\circ$ (*bottom*). The curves are the location of analytically calculated periodic orbits with $\Delta\dot{\varpi} = 0$. The lighter regions indicate regular oscillation of $\Delta\varpi$ (around 0 or 180°), whereas the darker regions indicate its regular circulation. The domains, where planetary collisions occur within 0.5 Myr, are hatched.

Figure 8. Same as in Fig. 6, but for $I_{\text{mut}} = 45^\circ$. The blue curves are the location of analytically calculated periodic orbits with $\dot{\omega}_1 = 0$, while the red curves of orbits with $\Delta\dot{\varpi} = 0$.

Figure 9. Dynamical map of the region around the v Andromedae system on the (a_2, e_2) -plane

of initial semimajor axis and eccentricity of the outer planet D. The high-order mean motion resonances are labeled on the top of the graph. The domains, where planetary collisions occur within 0.5 Myr, are hatched. The current position of the ν Andromedae system indicated by star symbol.

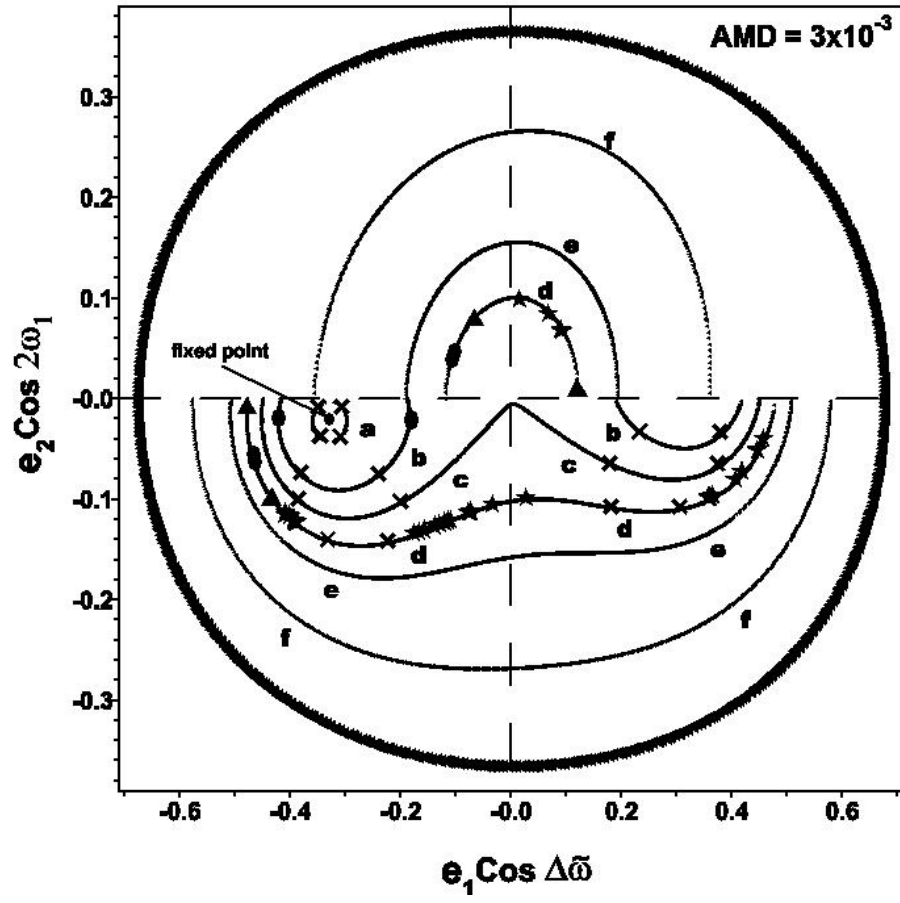


Figure 1: Michtchenko *et al.*

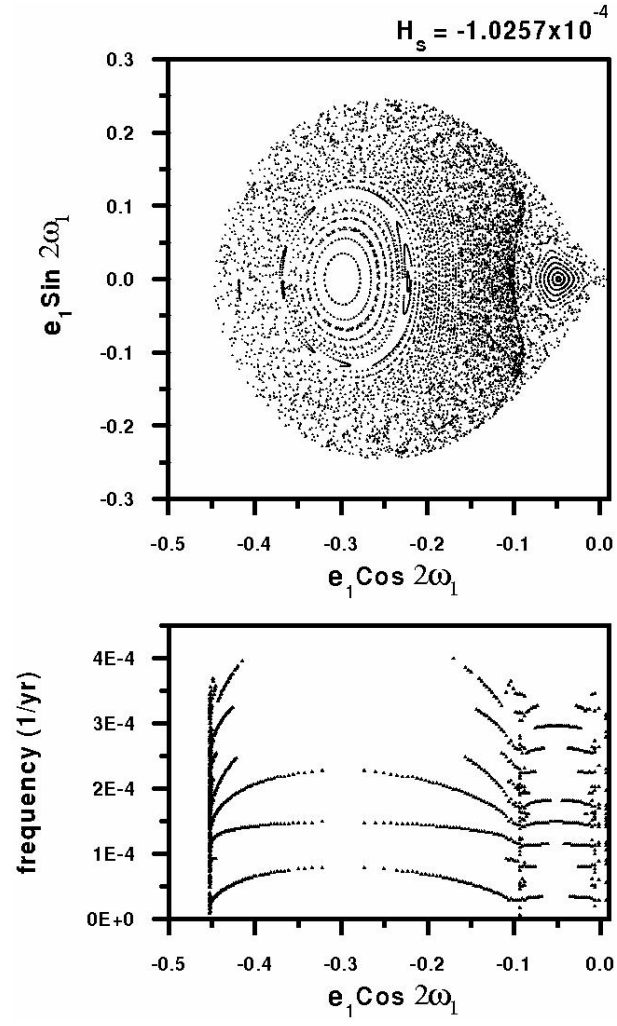


Figure 2: Michtchenko *et al.*

$$\text{AMD} = 3 \times 10^{-3}$$

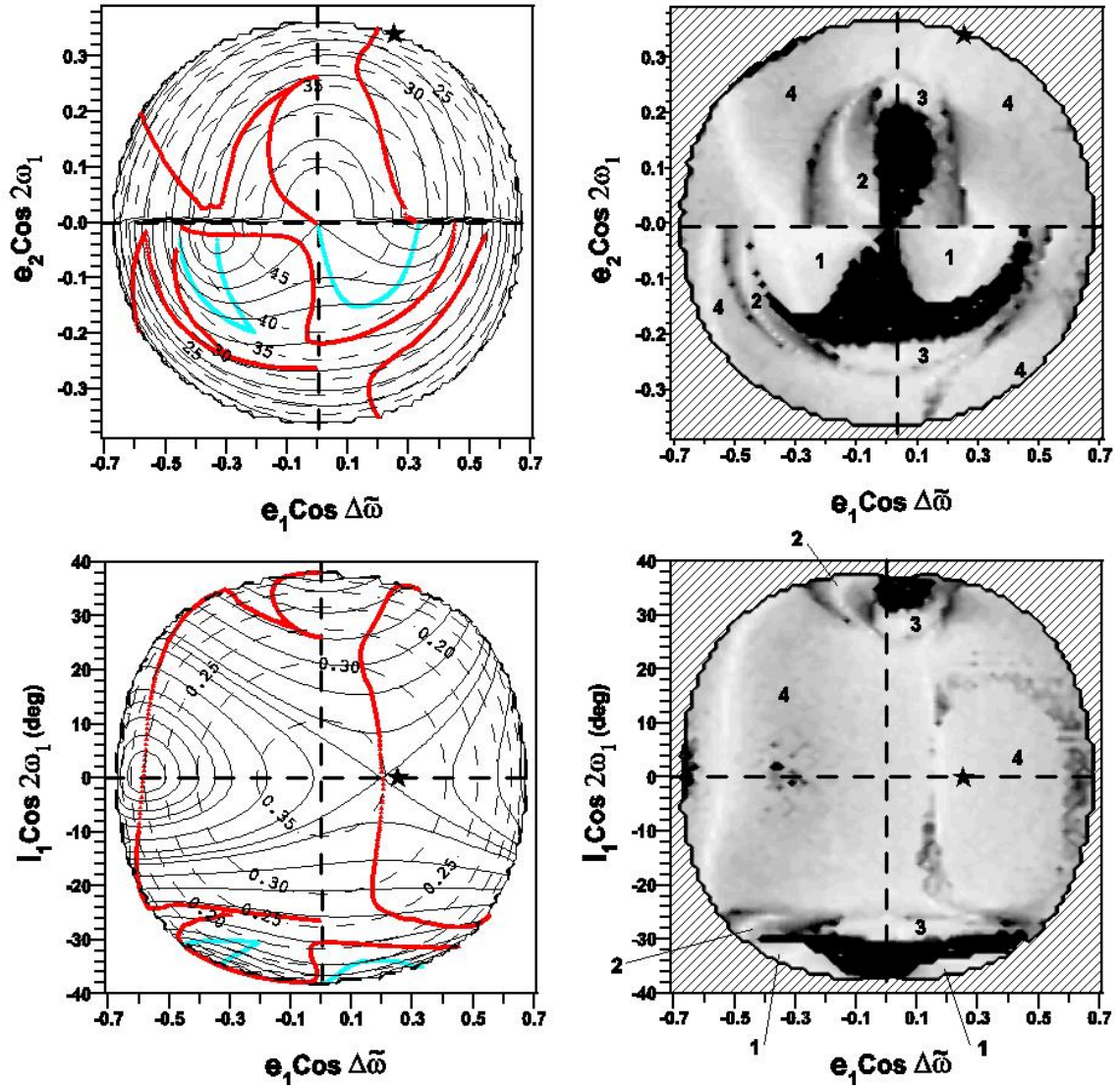


Figure 3: Michtchenko *et al.*

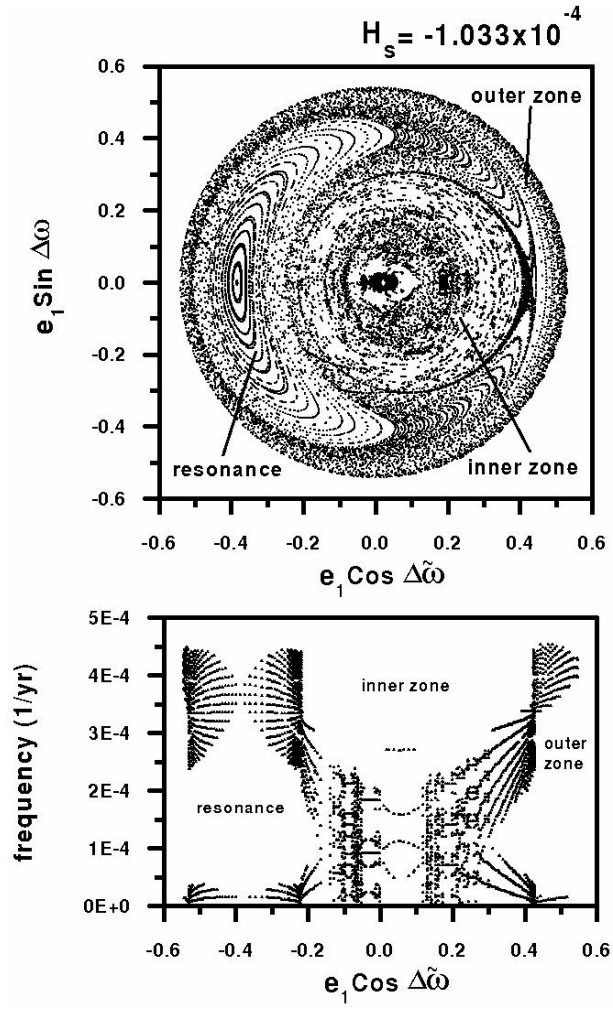


Figure 4: Michtchenko *et al.*

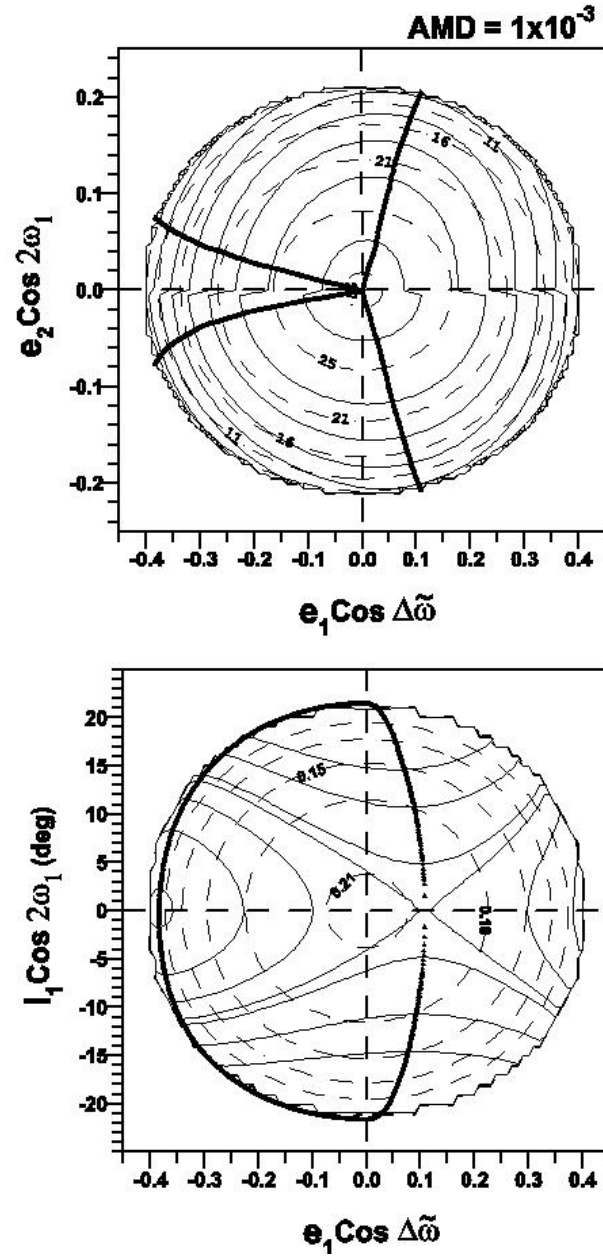


Figure 5: Michtchenko *et al.*

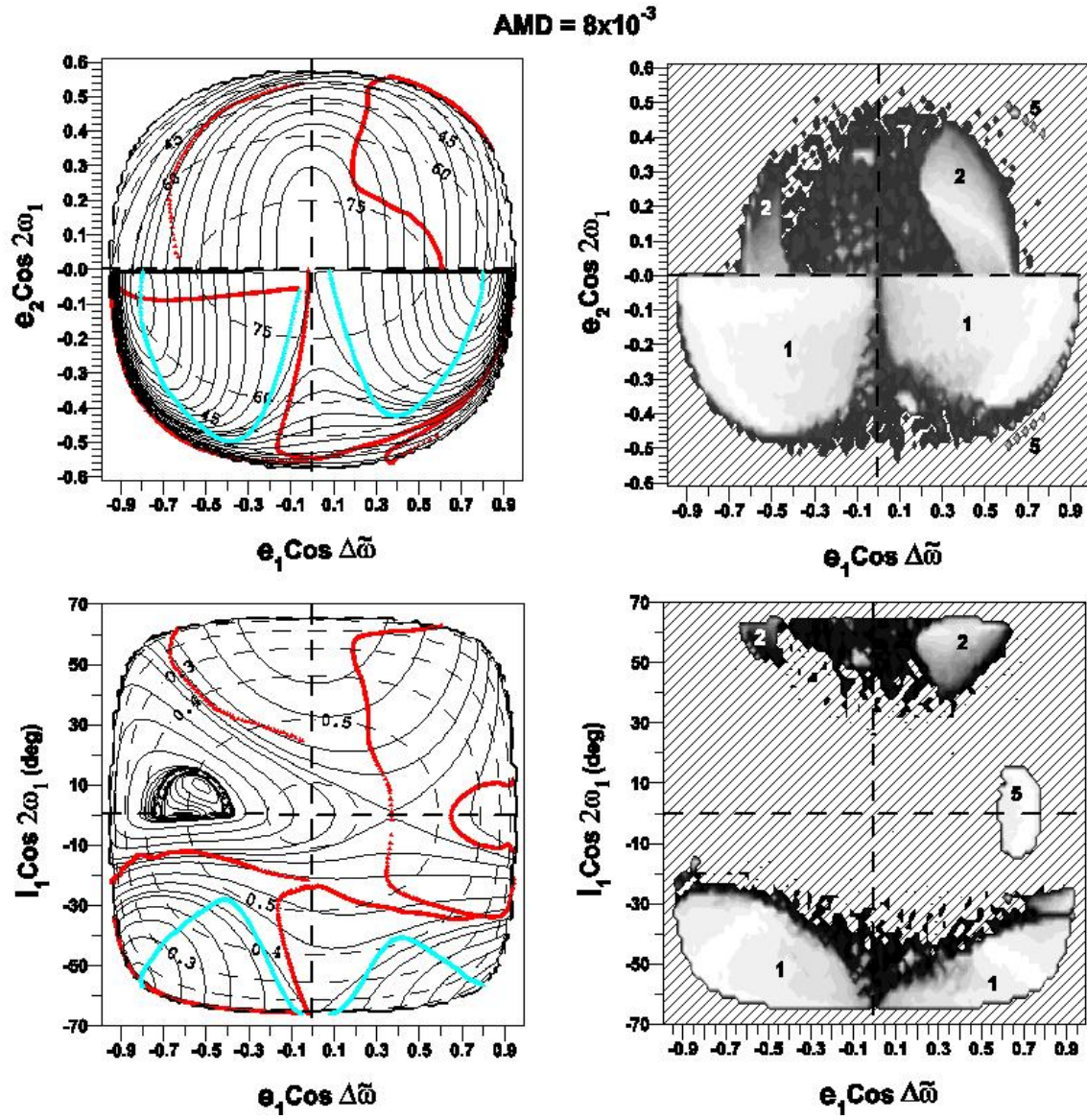


Figure 6: Michtchenko *et al.*

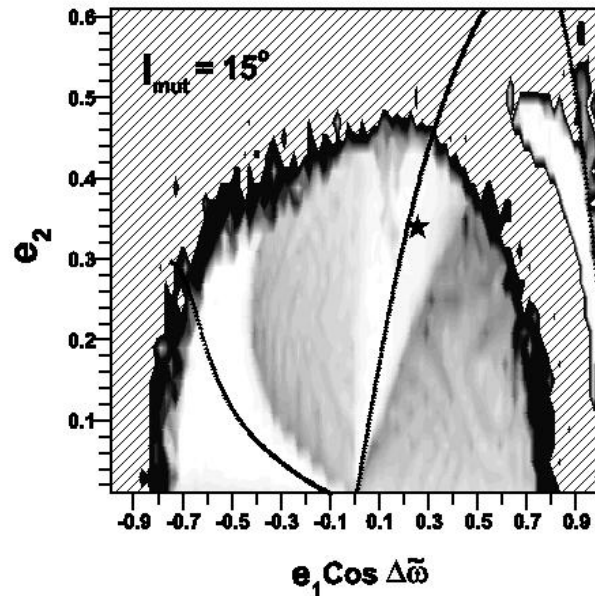
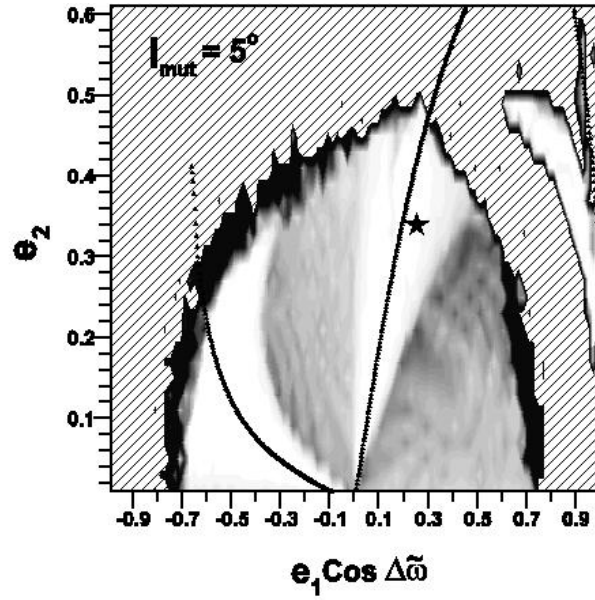


Figure 7: Michtchenko *et al.*

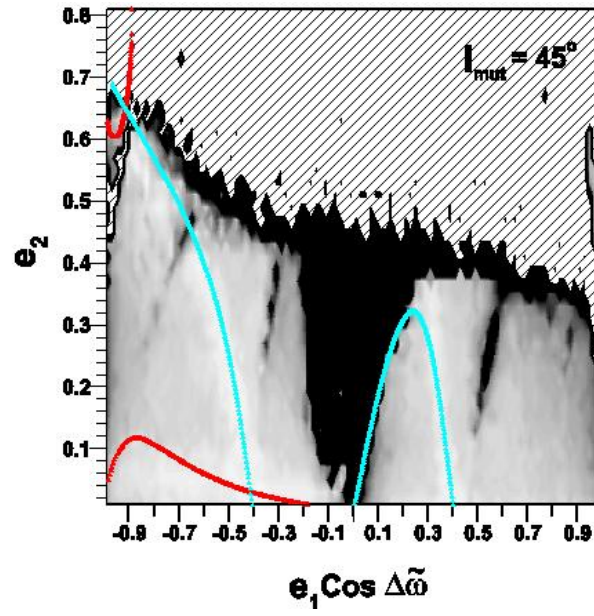


Figure 8: Michtchenko *et al.*

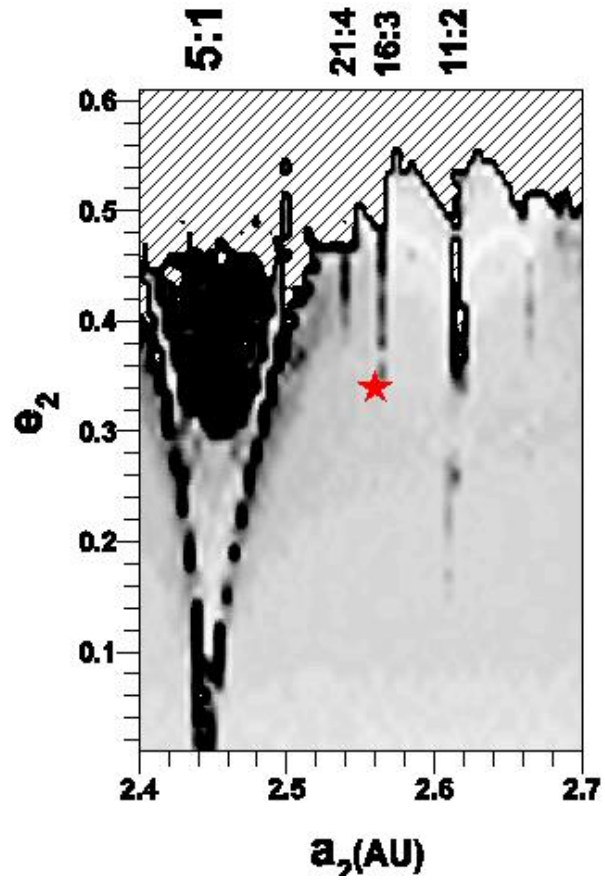


Figure 9: Michtchenko *et al.*